Article

Hydrogen Storage in Zeolite-Like Hexacyanometallates: Role of the Building Block

L. Reguera, J. Balmaseda, C. P. Krap, M. Avila, and E. Reguera

J. Phys. Chem. C, **2008**, 112 (44), 17443-17449• DOI: 10.1021/jp802764v • Publication Date (Web): 14 October 2008

Hydrogen Storage in Zeolite-Like Hexacyanometallates: Role of the Building Block

L. Reguera,[†] J. Balmaseda,[‡] C. P. Krap,[§] M. Avila,[§] and E. Reguera*[,§,⊥]

Universidad de La Habana, Cuba; Universidad Nacional Autónoma de México (UNAM), México; Instituto Politécnico Nacional, México, and Universidad de La Habana, Cuba.

Received: March 31, 2008

Hydrogen storage in zeolite-like hexacyanometallates, $Zn_3A_2[M(CN)_6]_2$ with A = K, Rb, Cs, and M = Fe, Ru, Os, was studied. In a previous article, we have reported the role of the exchangeable metal (A) for M = Fe on the H_2 adsorption. This contribution concerns to the effect of the molecular block, $[M(CN)_6]$, on the recorded H_2 adsorption isotherms and the corresponding adsorption heats. This family of porous materials can be considered as octahedral anionic blocks, $[M(CN)_6]^{4-}$, assembled by zinc (2+) atoms linked at their nitrogen ends. The porous framework topology was described from the refined crystal structures. In the resulting 3D network the zinc atom is found with a tetrahedral coordination. This leads to formation of ellipsoidal cavities, of about 12.5 × 9 × 8 Å, which remain communicated by elliptical windows. The H_2 adsorption heat was estimated using the isosteric method from isotherms recorded at 75 and 85 K. The estimated values for the adsorption heats follow the order: Os > Ru > Fe. The building block contribution to the H_2 adsorption potential takes place through the charge delocalization from the inner metal (M) to increase the electric field gradient at the cavity surface. The CO_2 adsorption isotherms are also conclusive on the contribution of the building block to the cavity adsorption potential. All of the studied samples were characterized from X-ray diffraction, infrared, and thermogravimetric data.

1. Introduction

The progress of human civilization is closely related to the availability of energy sources. From the first industrial activity for exploitation of petroleum, in 1859,[1] and then its processing to obtain different derivatives, practically all of the known technological advances have been linked to the use of this fossil fuel. Petroleum and other fossil fuels are nonrenewable energy resources, and for the next decades a definitive decline in their availability and production are expected. In addition, the combustion of fossil fuels leads to CO_2 emission, which is responsible for the global warming and of the related climate changes.[2] From these facts, the research and development activities on renewably energy sources have received increasing attention in the last decades. In this sense, sunlight harvesting appears to be most attractive solution.[3] However, for applications like automotive vehicles, and also as an energy storage medium, a secondary energy bearer is required. Hydrogen is a promising secondary-energy bearer related to its clean combustion (produces water as byproduct) and high heating value (572 kJ/mol). For such applications, the main fundamental and technological challenge is to find appropriate methods for hydrogen storage. Hydrogen, in its molecular form, H_2, can only be maintained in liquid state below 32.7 K (the H_2 critical temperature), independent of the applied pressure, and the liquefaction process consumes about 40% of the energy to be generated. H_2 storage at high pressure appears to be impractical, for a pressure of 345 atm. a density of 15/g is obtained, relatively low compared with 70 g/L for liquid state. Regarding the hydrogen storage for vehicular applications, the U.S. Department of Energy (DOE) has set a series of targets, nowadays worldwide accepted as reference targets, which include a gravimetric storage capacity of at least 9 wt % (2015 target), and with an appropriate adsorption−desorption kinetics at temperatures below 373 K to allow a quick and safe refueled process.[4]

The highest hydrogen storage capacity has been reported through the use of chemical and metal hydrides but, with these materials, the hydrogen desorption usually requires of high temperatures (>500 K) and the reversibility is not always guaranteed.[5] These features are the main handicap of these storage media. An attractive option is the physical adsorption due to its reversibility, but with the inconvenience, to date, of relatively low gravimetric density of adsorbed hydrogen.[6] Several families of porous materials have been evaluated for hydrogen storage, among them, carbon-based materials,[7] zeolites,[8] and metal-organic frameworks.[9−11] For zeolites, the presence of exposed highly polarizing cations in channels and cavities has been related to the possibility of attaining an appropriate stabilization for the hydrogen molecule within the microporous structure.[6,8,12] More recently, cyanide-based porous coordination polymers have received certain attention as a prototype of materials for hydrogen storage.[13−24] The relatively high ability that these last materials show for the hydrogen storage has been attributed to the availability of free coordination sites for the nitrogen-bound metal site at the pores' surface, in their anhydrous phases, and/or to an appropriate electric field gradient within the cavity.[13−23] From a recent study, we have reported on the role of the exchangeable alkali metal for the H_2 storage in zeolite-like hexacyanoferrates (II), $Zn_3A_2[Fe(CN)_6]_2$ (A = K, Rb, Cs).[21] However, to the best of our knowledge, the effect of the building block on the H_2 adsorption potential in this family of materials has not been reported. The H_2 adsorption isotherms at 75 and 85 K were now recorded for $Zn_3A_2[M(CN)_6]_2$ with M = Fe, Ru, Os. The estimated values

* To whom correspondence should be addressed. E-mail: ereguera@yahoo.com.
[†] Facultad de Química.
[‡] Departamento de polímeros, Instituto de Investigaciones en Materiales, México, D.F. C.P. 04510.
[§] Centro de Investigación en Ciencia Aplicada y Tecnología Avanzada-Unidad Legaria.
[⊥] Instituto de Ciencia y Tecnología de Materiales.

10.1021/jp802764v CCC: $40.75
Published on Web 10/14/2008

for the adsorption heats follow the order Os > Ru > Fe, suggesting that the building block effectively contributes to the adsorption potential for H_2 in this family of materials. This evidence is also supported by the recorded CO_2 adsorption data. A discussion on the nature of such contribution is provided. All of the samples to be studied were characterized from X-ray diffraction (XRD), infrared (IR), and thermogravimetric (TG) data.

2. Experimental Section

Hot aqueous solutions (0.01 M) of zinc chloride and $K_4[M(CN)_6]\cdot 3H_2O$ with M = Fe, Ru, Os, were mixed and the resulting precipitate separated after 2 days of aging within the mother liquor at the temperature of precipitation (333 K). The obtained solid was washed several times with distilled water until to obtain a solution free of chloride, according to the silver precipitate test. Then the solid was dried in air until it had a constant weight. The nature of the solids as hexacyanometallates was confirmed from IR spectra. The metals atomic ratio in the samples was estimated from X-ray energy-dispersed spectroscopy (EDS) analyses, using a spectrometer (from Noran Co.) coupled to a scanning electron microscope (SEM) (from Jeol Co.). The hydration degree (number of water molecules per formula unit) was estimated from TG curves. The compounds containing rubidium and cesium as exchangeable metals were prepared through ionic exchange from $Zn_3K_2[M(CN)_6]_2\cdot xH_2O$ in aqueous solutions at 333 K, according to a reported procedure.[25] The ionic exchange process was monitored from EDS analyses for the involved alkali metals. Potassium hexacyanoruthenate(II) and hexacyanoosmate(II) used were prepared from $RuCl_2\cdot H_2O$ and OsO_4 and KCN according to procedures indicated in the Supporting Information. The nature and purity of all of the intermediate and end products were tested by IR spectroscopy and XRD measurements. The structural characterization of the samples to be studied was carried out from IR and XRD data.

A high-resolution TA Instrument (Hi-ResTM) thermo-gravimetric analyzer TGA 2950 and instrument control software Thermal Advantage version 1.1A were used to measure the weight loss profiles for the studied samples. The TGA 2950 was used in dynamic rate mode where the heating rate is varied dynamically according to a ramp in response to the derivative of weight change (as derivative increases, heating rate is decreased and vice versa). The heating rates were constrained to be at the 0.001 to 5 K/min range with an instrumental resolution of 5. The furnace purge was nitrogen using flow rates of 100 mL/min. IR spectra were collected using an FTIR spectrophotometer (Spectrum One, from PerkinElmer) and the KBr pressed disk technique. XRD powder patterns were recorded in Bragg−Brentano geometry by means of a D5000 diffractometer (from Siemens) and monochromatic Cu Kα radiation, from 5 to 110 °(2θ), at a step size of 0.025 and 25 s of counting time. The structural refinement from the obtained XRD powder patterns was carried out with the Fullprof 2005 code[26] and pseudo-Voigt peak shape lines. Peak profiles were calculated within 10 times the half-line width. The background was modeled through third order polynomial fitting.

The CO_2 and H_2 adsorption isotherms were recorded using ASAP 2020 analyzer (from Micromeritics). Sample tubes of known weight were loaded with 40−50 mg of sample and sealed using TranSeal. Previous to the CO_2 or H_2 adsorption, the samples were degassed on the ASAP analyzer using a heating rate of 1 K/min and then maintained at the dehydration temperature indicated by the TG curve until to obtain a stable outgas rate below 10^{-6} Torr. The degassed sample and sample tube were weighed and then transferred back to the analyzer with the TranSeal preventing exposure of the sample to air. After volume measurement with helium, the degassing was continued for 24 h at 353 K in the sample port. Measurements were performed at 75 and 85 K using liquid N_2 and argon baths for H_2, and at 273 K for CO_2. These relatively low temperatures for liquid N_2 (75 K) and argon (85 K) are related to the local atmospheric pressure, 586 Torr.

The hydrogen adsorption isotherms were evaluated according to Langmuir−Freundlich (LF) equation based on the vacancy solutions theory:[27]

$$P_{eq} = P_{0.5}\left(\frac{n_{ad}}{n_p - n_{ad}}\right)^g \quad (1)$$

In eq 1, n_{ad} is the amount adsorbed at the equilibrium pressure, P_{eq}, n_p is the limiting amount filling the micropores, and $P_{0.5}$ is the equilibrium pressure at $n_p/2$, and g is the osmotic coefficient of the solution of vacancies and adsorbates and are related to the solution deviation from ideality. The value of g can be used as sensor for the strength of the guest−host interaction.[21−23]

As will be discussed below, the recorded CO_2 adsorption isotherms correspond to two adsorption domains. The domain of low relative pressure values was fitted according to the Langmuir model,[28]

$$n_{ad} = n_p K_L P_{eq}/(1 + K_L P_{eq}) \quad (2)$$

where K_L is the Langmuir constant. In eq 2, n_p represents the limiting amount occupying the adsorbate monolayer.

In the adsorption domain of higher relative pressures, the recorded isotherm corresponds to the pore volume filling, and it was fitted using the Dubinin−Astakhov (DA) equation,[29]

$$n_{ad} = n_p \exp\left\{-\left[\frac{RT}{E_0}\ln(P_r^{-1})\right]^n\right\} \quad (3)$$

where $P_r = P_{eq}/P_v$ is the relative pressure; E_0 is the characteristic energy; n is the heterogeneity parameter; R is the universal gas constant; and T is the temperature.

The enthalpy of adsorption (ΔH_{ads}) was obtained by the isosteric method from isotherms recorded at two temperatures and then using a variant of the Clasius−Clapeyron equation to calculate the ΔH_{ads} value according to the following:[28]

$$\ln\left(\frac{P_1}{P_2}\right) = \frac{\Delta H_{ads}}{R}\frac{T_2 - T_1}{T_1 T_2} \quad (4)$$

3. Results and Discussion

3.1. Structural Characterization of the Materials to be Studied. For the ruthenium and osmium series, the materials under study were found to be isomorphous with their iron analogues,[30] crystallizing with a rhombohedral unit cell ($R\bar{3}c$). In Table 1, the estimated cell parameters for all the series are collected. The corresponding XRD powder patterns, experimental, and fitted, and the refined crystal structures are available in the Supporting Information. As starting structural model to be refined, the reported structure for $Zn_3K_2[Fe(CN)_6]_2\cdot xH_2O$ was taken.[31] This structure provided the initial positions for the framework atoms. The interatomic C−N distance was constrained to take values within certain limits considering results from single crystal studies in analogue compositions.[25,31,32] The crystal structure of these series of zinc compounds can be considered as the assembling of MC_6 octahedra and ZnN_4 tetrahedra to form a porous 3D framework (Figure 1). It can also be regarded as $M(CN)_6$ octahedral blocks bridged by zinc

TABLE 1: Formula Unit, Unit Cell Parameters, ν(CN) and ν(M−C) Frequencies, and the Estimated Dehydration Temperature

formula unit	cell parameters[a], [Å]	ν(CN), [cm^1]	ν(M−C), [cm^1]	dehyd. temp., [K]
$Zn_3K_2[Fe(CN)_6]_2\cdot 6.8H_2O$	$a = b = 12.5409(3)$, c=32.158(1)	2100	493	436
$Zn_3K_2[Ru(CN)_6]_2\cdot 6H_2O$	$a = b = 12.8759(1)$, $c = 32.6814(6)$	2103	481	327
$Zn_3K_2[Os(CN)_6]_2\cdot 5.6H_2O$	$a = b = 12.8709(5)$, $c = 32.6447(6)$	2089	496	319
$Zn_3Rb_2[Fe(CN)_6]_2\cdot 6.8H_2O$	$a = b = 12.5013(2)$, $c = 32.512$ (1)	2099	494	390
$Zn_3Rb_2[Ru(CN)_6]_2\cdot 6H_2O$	$a = b = 12.8296(5)$, $c = 33.0563(1)$	2104	482	387
$Zn_3Rb_2[Os(CN)_6]_2\cdot 5.6H_2O$	$a = b = 12.8289(2)$, $c = 32.9920(5)$	2090	504	385
$Zn_3Cs_2[Fe(CN)_6]_2\cdot 6.8H_2O$	$a = b = 12.4841(3)$, $c = 32.832(4)$	2098	491	370
$Zn_3Cs_2[Ru(CN)_6]_2\cdot 6H_2O$	$a = b = 12.8046(4)$, $c = 33.3931(5)$	2101	478	368
$Zn_3Cs_2[Os(CN)_6]_2\cdot 5.6H_2O$	$a = b = 12.7830(7)$, $c = 33.5318(1)$	2090	507	366

[a] In a hexagonal cell representation.

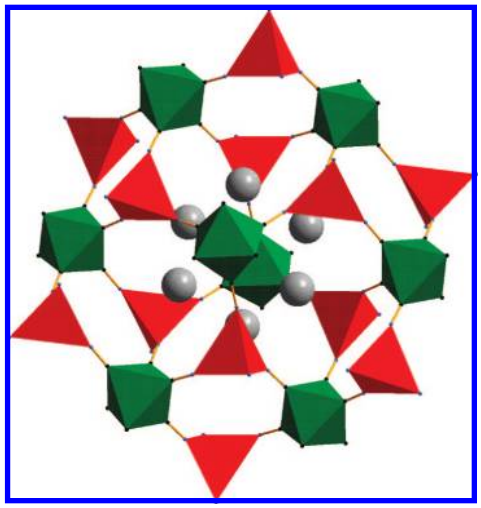

Figure 1. Framework of the materials under study. The exchangeable alkali metals located close to the ZnN_4 polyhedron corners are indicated with small spheres. That position for the alkali metal corresponds to the estimated coordinates for a hydrated material with five water molecules per formula unit.

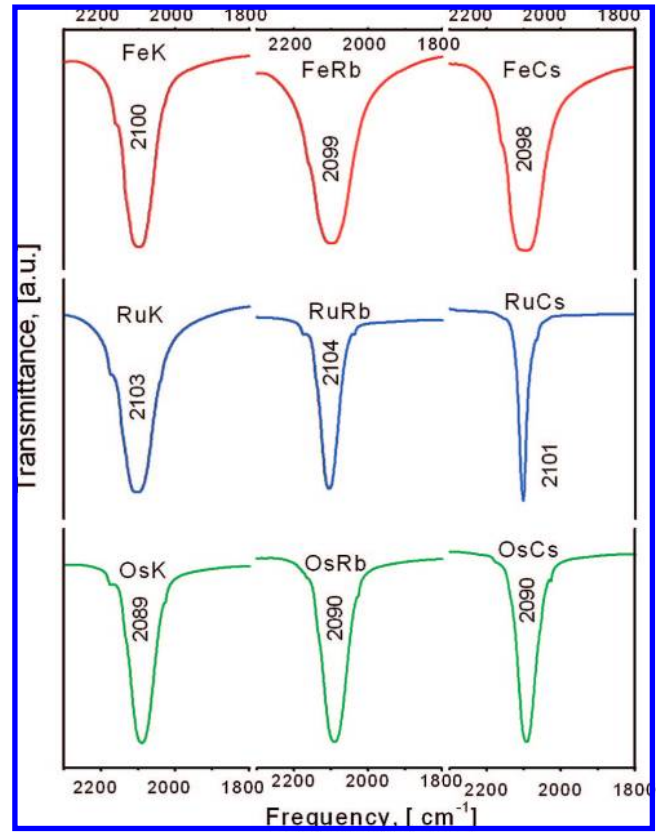

Figure 2. IR spectra (the ν(CN) stretching region only) for the studied series of zeolite-like zinc hexacyanometallates (II). Indicated is the ν(CN) frequency.

atoms tetrahedrally coordinated at their nitrogen ends. The synthesis process corresponds to this second option. During the zinc salt formation, the building unit, $[M(CN)_6]$, approximately preserves its original geometry; however, the N−Zn−N bond deviates from the linearity. On average, the N−Zn−N angle was estimated to be 108°. The formation of windows of elliptical shape and also of ellipsoidal cavities is related to such deviation from linearity. Each of these cavities, of ca. 12.5 × 9 × 8 Å, remains communicated by six elliptical windows of about 6 Å of larger diameter (Figure 1). This cavity geometry has been confirmed by ^{129}Xe NMR spectra.[33] At the surface of a given cavity, 8 octahedra and 12 tetrahedra are found, and because these building units are shared by a neighboring cavity, the amount of formula units per cavity is 2. The exchangeable or charge balancing ion (A) is located close the cavity windows, near to the ZnN_4 corners (in hydrated samples). This is probably related to certain concentration of electric field gradient in that region due to the local deformation around the zinc atom together with the excess of negative charge from the anion. However, for different hydration degree related to the involved alkali ion (A^+) deviations from such position are found,[25,31,32] suggesting that the cation has certain mobility within the cavity and its equilibrium position probably depends on the nature and amount of adsorbed species.

The IR spectrum is a good structural sensor for hexacyanometallates. The ν(CN) band frequency senses the valence, electronic configuration, and coordination number of the metals bonded at the carbon and nitrogen ends of the CN ligands.[34] For iron and ruthenium, this vibration was observed around 2100 cm^{-1}, and at 10 cm^{-1} lower frequency (2090 cm^{-1}) for osmium (Figure 2, Table 1). For analogue families of manganese and cadmium hexacyanometallates(II), also the lower frequency for the ν(CN) vibration is found for the osmium series.[35] In hexacyanometallates, the metal t_{2g} orbitals and the π^* orbitals of the CN groups are in appropriate space disposition to allow their partial overlapping. These orbitals have similar energy, which also facilitates the charge transfer among them. From these features, the well-known metal to ligand π-back charge donation in hexacyanometallates results. This is sensed in the IR spectrum as a decrease for the ν(CN) frequency.[36] The relatively low ν(CN) frequency observed for the osmium series (Figure 2) is caused by a strong π-back donation from the osmium atom. Compared with iron and ruthenium, osmium shows a better ability to the back-bonding interaction because third-row metals have more diffuse d orbitals. The π-back-donation leads to a relatively large concentration of charge on the CN group, which is probably localized on the nitrogen end. The well-known magnetic ordering in transition metals hexacya-

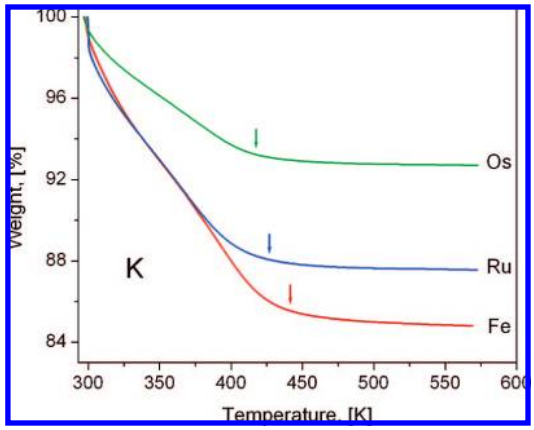

Figure 3. TG curves (dehydration region) for $Zn_3K_2[M(CN)_6]_2 \cdot xH_2O$; M = Fe, Ru, Os. Similar TG curves were obtained for A = Rb and Cs. The arrows indicate the dehydration temperature which follows the order Os < Ru < Fe.

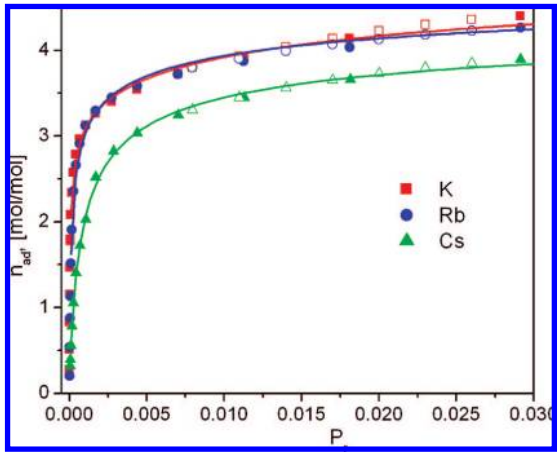

Figure 4. CO_2 adsorption isotherms for the ruthenium series, $Zn_3A_2[Ru(CN)_6]_2$ with A = K, Rb, Cs. These isotherms were fitted using a combination of Langmuir and Dubinin−Astakhov models.

nometallates is conclusive in that sense. The charge removed from the inner metal through the π-back bonding interaction is placed on the nitrogen end, and this makes possible the metals electronic cloud overlapping.[37−39] The π-back bonding interaction leads to a stronger M−CN bond. In the IR spectrum, this is observed as a frequency blue shift for the ν(M−C) vibration. To the osmium series belong the largest ν(M−C) frequency shifts (Table 1).

Figure 3 shows the TG curves for $Zn_3K_2[M(CN)_6]_2 \cdot xH_2O$ with M = Fe, Ru, Os. Similar sets of TG curves were obtained for rubidium and cesium (see Supporting Information). The temperature value where the sample becomes anhydrous shows a gradual low-temperature shift. This temperature shift follows the order Os > Ru > Fe. This corresponds to a weaker interaction for the alkali metal with the coordinated waters, the last ones to be evolved. A stronger interaction of the alkali metal (A) with the cavity surface, through the mentioned charge delocalization, causes a decrease for its effective polarizing power, and a weaker interaction with the coordinated waters results. This is sensed as a lower dehydration temperature.

3.2. Carbon Dioxide Adsorption Data. Figure 4 shows the CO_2 adsorption isotherms for the ruthenium series. Analogue isotherms were observed for iron and osmium series (Supporting Information). According to these isotherms, the maximum amount adsorbed filling the pore volume follows the order K > Rb > Cs. This behavior is analogue to the previously

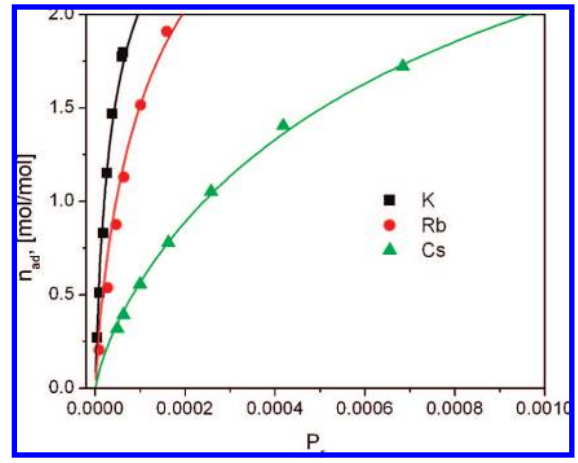

Figure 5. Low-pressure region of the CO_2 adsorption isotherms for the Ru series, $Zn_3A_2[Ru(CN)_6]_2$ with A = K, Rb, Cs. That region was fitted using the Langmuir model.

observed for the iron series.[21] The exchangeable metal occupies a fraction of the cavity volume reducing the available volume for the CO_2 adsorption. To the bigger metal, cesium, the lower maximum adsorption corresponds.

In the recorded CO_2 adsorption isotherms, two adsorption domains were appreciated. The adsorption in the low pressures region can be fitted according to the Langmuir model as shown in eq 2. Figure 5 shows the fitting of that region for the ruthenium series. That region corresponds to a maximum adsorption of 2 mol/mol. This is equivalent to a CO_2 molecule per exchangeable metal (A), the monolayer of CO_2 adsorbed on the metal. The isotherm slope in that region follows the order K > Rb > Cs, suggesting that the adsorption potential is dominated by the electrostatic interaction between the metal polarizing power and the adsorbate quadrupole moment. Such dependence was already observed for the iron series.[21]

The CO_2 adsorption isotherms were fitted as a whole through a combination of eqs 2 and 3, limiting the fitting according to eq 2 for the region below 2 mol/mol. The estimated values for the Langmuir constant (K_L) and the DA model parameters are collected in Table 2. In accordance with the qualitative evaluation of the recorded isotherms at low pressures, the K_L values follow the order K > Rb > Cs for all of the series. For a given cation and different building blocks, no definite trend was observed (Table 2). The adsorption potential in that region is dominated by the electrostatic interaction between alkali metal and the CO_2 molecule, probably shielding any contribution from the building block (discussed below).

In the DA model, the heterogeneity parameter (n) indicates the heterogeneity sensed by the probe molecule for the adsorption potential. A large n value corresponds to an adsorption potential with low heterogeneities. According to the obtained values for this parameter (n) (Table 2), as bigger and less polarizing is the metal found within the cavity, a more homogeneous adsorption potential is sensed by the CO_2 molecule. This adsorption domain corresponds to molecules that are adsorbed at increasing distance from the alkali metal, and in consequence, sensing a weaker and variable electric field gradient. For potassium, the most polarizing metal within the studied series, the larger variation in that local adsorption potential is expected and really sensed as the smaller n value. By the same reason, to cesium the less heterogeneous potential corresponds. When the values of n are examined according to the involved building block, the heterogeneity for the adsorption potential follows the order Os > Ru > Fe. This was attributed

TABLE 2: Results Derived from the CO_2 Adsorption Isotherms Fitting According to a Combination of the Langmuir and Dubinin−Astakhov Models[a]

compound	K_L	E_o, [kJ/mol]	n_p, [mol/mol]	n	CO_2/cavity	wt [%]
$Zn_3K_2Fe_2$	0.97 ± 0.22	17.4 ± 0.2	4.4 ± 0.1	2.9 ± 0.1	8.8	29
$Zn_3Rb_2Fe_2$	0.29 ± 0.003	16.9 ± 0.3	3.8 ± 0.1	5.1 ± 0.7	7.6	22
$Zn_3Cs_2Fe_2$	0.172 ± 0.004	12.8 ± 0.4	3.1 ± 0.2	5.9 ± 1.6	6.2	16
$Zn_3K_2Ru_2$	1.09 ± 0.01	16.1 ± 0.7	4.2 ± 0.2	2.0 ± 0.2	8.4	25
$Zn_3Rb_2Ru_2$	0.34 ± 0.02	17.5 ± 0.2	4.0 ± 0.1	2.3 ± 0.1	8.0	21
$Zn_3Cs_2Ru_2$	0.155 ± 0.006	15.8 ± 0.4	3.5 ± 0.1	2.4 ± 0.2	7.0	16
$Zn_3K_2Os_2$	0.93 ± 0.02	11.2 ± 1.2	3.7 ± 0.2	1.4 ± 0.1	7.4	18
$Zn_3Rb_2Os_2$	0.61 ± 0.09	12.4 ± 1.8	3.6 ± 0.2	1.8 ± 0.4	7.2	15
$Zn_3Cs_2Os_2$	0.120 ± 0.001	13.6 ± 0.6	3.5 ± 0.2	2.5 ± 0.3	7.0	14

[a] K_L, the Langmuir constant; n_p, the limiting amount adsorbed filling the micropores; E_o, characteristic energy; n, heterogeneity parameter; and storage capacity in weight percent (wt %).

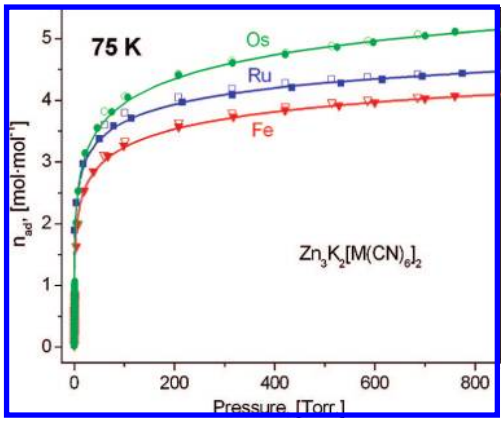

Figure 6. H_2 adsorption isotherms at 75 K for $Zn_3K_2[M(CN)_6]_2$, M = Fe, Ru, Os. For Rb and Cs series analogue behaviors were observed (Supporting Information).

to the charge accumulation on the cavity surface through the already-mentioned charge delocalization from the inner metal through the π-back-donation mechanism.

In the DA model, the characteristic energy (E_o) represents the average energy involved in the adsorption process. From this fact, the value of E_o can be used as a sensor for the guest−host interaction. According to the estimated E_o values (Table 2), for the iron series the order is K > Rb > Cs, which agrees with a previous study on these compounds.[21] However, for the osmium series the inverse order was found, Cs > Rb > K, whereas for ruthenium an intermediate behavior was noted (Table 2). This suggests that the building block is contributing to the adsorption potential within the cavity. This evidence is supported by the already-disccussed TG results.

3.3. Hydrogen Adsorption Isotherms. Figure 6 shows the recorded H_2 adsorption isotherms at 75 K for the K series, $Zn_3K_2[M(CN)_6]_2$ with M = Fe, Ru, Os. For rubidium and cesium series, analogue H_2 adsorption isotherms were recorded (Supporting Information). From their simple inspection, valuable qualitative information is obtained. The H_2 molecule senses a relatively strong adsorption potential within the cavity. At about 200 Torr, the recorded adsorption isotherms show evidence of saturation. The isotherms slope at low relative pressures follows the order of Os > Ru > Fe, suggesting that this is the order for the adsorption potential. This order suggests that the building block has a definite contribution to the H_2 adsorption. Analogue qualitative information is obtained from the adsorption isotherms recorded at 85 K (Supporting Information). In Table 3, the results obtained from the adsorption data fitting according to eq 1 are collected. For a given exchangeable metal, the limiting amount filling the micropores, n_p, follows the order: Os > Ru > Fe. The observed variation for the n_p value within the three series both at 75 and 85 K (Table 3) was ascribed to the available space in the cavity to accommodate H_2 molecules. Within the considered alkali metals, cesium is the bigger one and occupies an important fraction of the cavity volume. This explains the variation of the n_p value with the involved alkali metal.

In the LF model the estimated value for the osmotic coefficient (g) represents a sensor for the strength of the guest−host interaction.[27] We have found that this parameter results particularly useful in comparative studies for the H_2 storage within a given family of materials.[21−23] For $g = 1$, eq 1 is equivalent to the Langmuir model (eq 2), which supposes a mobile adsorbate without lateral interactions among the adsorbate particles, with all of them sensing the same adsorption potential.[40] A value of $g > 1$ represents a deviation from such ideal conditions. As expected, when the value of g for the adsorption isotherms recorded at 75 and 85 K are compared, to the formers the larger g values correspond (Table 2). At a lower adsorption temperature, the H_2 molecule senses a stronger adsorption potential and a more localized adsorption. For a given alkali metal, the value of g follows the order: Os > Ru > Fe, without exception, in correspondence with the above-discussed qualitative evidence from the isotherm slope at low pressures.

3.4. Hydrogen Adsorption Heats. Figure 7 shows the dependence of ΔH_{ad}, estimated according to eq 4, for the potassium series, $Zn_3K_2[M(CN)_6]_2$, at relatively low values of n_{ad}, where the adsorbate−adsorbate interaction contribution to the adsorption potential can be ignored. The obtained ΔH_{ad} values follow the order Os > Ru > Fe. The same order for the values of ΔH_{ad} was found for rubidium and cesium series (Supporting Information). The larger increase for ΔH_{ad} was observed between ruthenium and osmium compounds (Figure 7), a behavior analog to that observed from IR spectra (Figure 2 and Table 1). According to the ΔH_{ad} variation for a given alkali metal, the main contribution to the adsorption heats can be attributed to the cation effect but, with a detectable component from the building block. The building block contribution to the adsorption potential together with the available cavity free volume, determines the observed difference between the recorded isotherms for a given alkali metal.

Isosteric heats of H_2 adsorption have been reported for other families of cyanometallates, particularly in Prussian blue (PB) analogues with values in the 5−7.5 kJ/mol range.[13,16−18] In these compounds, the adsorption potential has been related to the metal centers of unsaturated coordination sphere located at the cavity surface. Such metal centers are responsible for the cavity electric-field gradient but also certain H_2-to-metal coordination type interaction could be present. [23] For the family of zinc hexacyanometallates(II), that last contribution is discarded because the zinc atoms have saturated their coordination sphere.

TABLE 3: Results Derived from the H_2 Adsorption Isotherms Fitting According to the Langmuir−Freundlich Model[a]

compound	temp., [K]	n_p, [mol/mol]	H_2/cavity	g	wt [%]	ΔH_{ad}, [kJ/mol]
$Zn_3K_2Fe_2$	75	5.8 ± 0.3	11.6	3.3 ± 0.3	1.66 ± 0.01	8.3
	85	4.5 ± 0.1	9	1.8 ± 0.2	1.29 ± 0.01	
$Zn_3K_2Ru_2$	75	6.0 ± 0.6	12	3.4 ± 0.7	1.5 ± 0.2	8.4
	85	5.1 ± 0.2	10.2	2.3 ± 0.2	1.29 ± 0.05	
$Zn_3K_2Os_2$	75	8.0 ± 1.0	16	3.6 ± 0.7	1.7 ± 0.2	8.6
	85	7.0 ± 0.6	14	2.8 ± 0.3	1.4 ± 0.1	
$Zn_3Rb_2Fe_2$	75	4.7 ± 0.1	9.4	1.80 ± 0.08	1.19 ± 0.01	6.8
	85	4.4 ± 0.2	8.8	1.33 ± 0.08	1.11 ± 0.05	
$Zn_3Rb_2Ru_2$	75	5.8 ± 0.7	11.6	2.8 ± 0.7	1.3 ± 0.2	7.2
	85	5.6 ± 0.4	11.2	1.8 ± 0.2	1.27 ± 0.09	
$Zn_3Rb_2Os_2$	75	7.5 ± 1.0	15	3.6 ± 0.9	1.4 ± 0.2	7.4
	85	5.9 ± 0.4	11.8	1.9 ± 0.2	1.11 ± 0.08	
$Zn_3Cs_2Fe_2$	75	4.19 ± 0.04	8.4	1.68 ± 0.05	0.95 ± 0.01	6.2
	85	3.52 ± 0.02	7.04	1.29 ± 0.03	0.79 ± 0.01	
$Zn_3Cs_2Ru_2$	75	5.6 ± 0.8	11.2	2.3 ± 0.4	1.11 ± 0.2	6.9
	85	4.5 ± 0.3	9	1.7 ± 0.2	0.92 ± 0.06	
$Zn_3Cs_2Os_2$	75	6.3 ± 0.6	12.6	2.5	1.1 ± 0.1	7.1
	85	4.5 ± 0.3	9	1.9 ± 0.2	0.78 ± 0.05	

[a] n_p, the limit capacity of micropores; g, the osmotic coefficient), H_2/Cavity, the estimated limit amount of H_2 molecules per cavity; and wt %, the maximum estimated adsorption in weight percent.

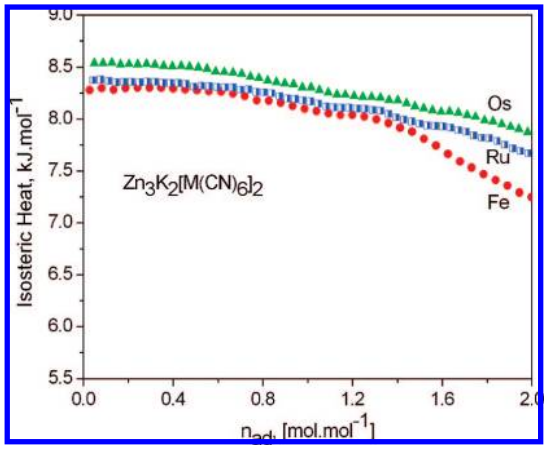

Figure 7. H_2 adsorption heat curves (the low adsorption region only) for $Zn_3K_2[M(CN)_6]_2$, M = Fe, Ru, Os. For rubidium and cesium series, analogue behavior was observed (Supporting Information).

In accordance with previous studies on the H_2 adsorption in porous cyanometallates,[21,22] in the studied family of zeolite-like porous solids the adsorption potential can be attributed to the electrostatic interaction between the cavity electric field gradient and the adsorbate quadruple moment, without discarding a small contribution from van der Waals type forces. Nevertheless, the estimated values for ΔH_{ad} are significantly larger, by about 30% (Table 3), than those reported for PB analogues.[13,16−18,23] The obtained dependence for the values of ΔH_{ad} on the involved building block parallels the variation observed for the estimated characteristic energies (E_o) in the CO_2 adsorption.

3.5. Nature of the Observed Building Block Effect on the H_2 Adsorption. As already-mentioned, in PB analogues the H_2 adsorption potential has been related to the existence of open metal sites at the cavities surface.[13−18] For the family of zinc hexacyametallates(II), $Zn_3A_2[M(CN)_6]_2$, no direct interaction between H_2 and the framework metals is possible because for these last ones the coordination sphere is saturated with CN groups. In this case, the adsorption potential must be attributed to an electrostatic interaction of the adsorbate (H_2) quadrupole moment with the electric field gradient at the cavity. The electric field gradient at the cavity has two contributions, the excess of negative charge on the molecular block and that from the alkali metal ion. The observed order, Os > Ru > Fe, for both ΔH_{ad} and the osmotic coefficient (g), suggests that the excess of the anion negative charge at the cavity surface depends on the involved inner metal, and for osmium the greater contribution to the cavity electric field gradient is detected.

From the study of the magnetic properties of PB analogues, it is well-known that in hexacyanometallates a large fraction of electronic density removed from the inner metal, through the π-back-donation mechanism, is located at the nitrogen end.[37−39] Such an effect depends of the metal linked at the carbon end. For a transition metal of the first-row, for example vanadium and chromium, with relatively large ionic radius and more diffuse d orbitals, the overlapping among the metal t_{2g} and ligand π^* orbitals is favored and a large charge delocalization results. In terms of the magnetic interaction, this is equivalent to a greater value for the integral of exchange (J) and a high temperature of magnetic ordering (T_c) results.[37,38] Within PB analogues, to these two metals highest values of T_c correspond.[38,41] From the above-discussed IR results for zinc hexacyanometallates(II) (Figure 2, Table 1), the lowest ν(CN) frequency value was found for osmium. This means that to this metal the greater charge delocalization within the materials under study takes place. The dehydration temperature shift observed from the TG curves also supports the charge delocalization according to Os > Ru > Fe. This explains the order Os > Ru > Fe for the H_2 adsorption potential sensed through the values of ΔH_{ad} and g, and also for the CO_2 adsorption using the characteristic energy (E_o) as sensor for the strength of the guest−host interaction. The charge-delocalization from the inner metal and its concentration on the cavity surface also contributes to understand the relatively high adsorption of H_2 in hexacyanometallates free of alkali metal within the cavity and without framework metals with unsaturated coordination sphere at the cavity surface; for instance, in the rhombohedral phase of zinc hexacyanocobaltate(III).[21]

The H_2 adsorption isotherms were also recorded at 273 K (Supporting Information). The H_2 adsorption potential close to room temperature resulted very weak, with a maximum adsorption about 0.2 mol/mol. In that sense, the above-discussed results must be considered of basic nature, to obtain information on the contribution of the building unit to the H_2 adsorption in this family of porous materials.

Conclusions

In zeolite-like zinc hexacyanometallates(II), the adsorption potential for H_2 mainly results from the electrostatic interaction among the hydrogen molecule quadrupole moment and the cavity electric field gradient. Both the alkali metal ion located within the cavity and the building block contribute to the cavity electric field gradient. The building block contribution is related to the π-back-donation at the carbon end and the corresponding charge delocalization from the inner metal (M) increasing the electronic density at the nitrogen end, on the cavity surface. As the charge delocalization gets stronger (the π-back-donation), the building block contribution to the H_2 adsorption potential gets larger. For the studied family of compounds, that contribution follows the order Os > Ru > Fe. To the best of our knowledge, this study represents the first experimental evidence of the building block effect on the hydrogen adsorption in porous hexacyanometallates. The results herein discussed for zeolite-like hexacyanometallates(II) shed light on possible routes to increase the adsorption potential for H_2 in porous solids.

Acknowledgment. L.R. acknowledges the support provided by the ALFA Project NANOGASTOR for her Ph.D. studies. This research was partially supported by the Project SEP-CONACyT-2007-61541. The authors thank E. Fregoso-Israel from IIM−UNAM for the TG data collection.

Supporting Information Available: Structural information has been deposited at ICSD Fachinformationszentrum Karlsruhe (FIZ) (e-mail: crysdata@fiz-karlsruhe.de) with CSD file numbers: 419319: $Zn_3K_2[Ru(CN)_6]_2 \cdot xH_2O$; 419320: $Zn_3K_2[Os(CN)_6]_2 \cdot xH_2O$; 419321: $Zn_3Rb_2[Ru(CN)_6]_2 \cdot xH_2O$; 419322: $Zn_3Rb_2[Os(CN)_6]_2 \cdot xH_2O$; 419323: $Zn_3Cs_2[Ru(CN)_6]_2 \cdot xH_2O$; 419324: $Zn_3Cs_2[Os(CN)_6]_2 \cdot xH_2O$. Supporting Information on the synthesis, XRD powder patterns, and TG curves for the materials under study and their CO_2 and H_2 adsorption isotherms. This material is available free of charge via the Internet at http://pubs.acs.org.

References and Notes

(1) Dunn, S. *Int. J. Hydrogen Energy* **2002**, *27*, 235.
(2) Idso, S. B. *Clim. Res.* **1998**, *10*, 69.
(3) Kamat, P. V. *J. Phys. Chem. C* **2007**, *111*, 2834.
(4) Hydrogen Storage. 2007 DOE Hydrogen Program. Merit Review and Peer Evaluation Meeting, U.S. Department of Energy. http://www.hydrogen.energy.gov/.
(5) Janot, R.; Eymery, J. B.; Tarascon, J. M. *J. Phys. Chem. C* **2007**, *111*, 2335.
(6) Torres, F. J.; Vitillo, J. G.; Civalleri, B.; Ricchiardi, G.; Zecchina, A. *J. Phys. Chem. C* **2007**, *111*, 2505.
(7) Bhatia, S. K.; Myers, A. L. *Langmuir* **2006**, *22*, 1688.
(8) Torres, F. J.; Civalleri, B.; Terentyev, A.; Ugliengo, P.; Pisani, C. *J. Phys. Chem. C* **2007**, *111*, 1871, and references therein.
(9) Rosi, N. L.; Eckert, J.; Eddaoudi, M.; Vodak, D. T.; Kim, J.; O'Keeffe, M.; Yaghi, O. M. *Science* **2003**, *300*, 1127.
(10) Sun, D.; Ma, S.; Ke, Y.; Collins, D. J.; Zhou, H.-C. *J. Am. Chem. Soc.* **2006**, *128*, 3896.
(11) Kaye, S. S.,; Dailly, A.; Yaghi, O. M.; Long, J. R. *J. Am. Chem. Soc.* **2007**, *129*, 14176, and references therein.
(12) Vitillo, J. G.; Damin, A.; Zecchina, A.; Ricchiardi, G. *J. Chem. Phys.* **2006**, *124*, 224308.
(13) Kaye, S. S.; Long, J. R. *J. Am. Chem. Soc.* **2005**, *127*, 6506.
(14) Chapman, K. W.; Southon, P. D.; Weeks, C. L.; Kepert, C. J. *Chem. Commun.* **2005**, 3322.
(15) Hartman, M. R.; Peterson, V. K.; Liu, Y.; Kaye, S. S.; Long, J. R. *Chem. Mater.* **2006**, *18*, 3221.
(16) Culp, J. T.; Matranga, C.; Smith, M.; Bittner, E. W.; Bockrath, B. *J. Phys. Chem. B.* **2006**, *110*, 8325.
(17) Kaye, S. S.; Long, J. R. *Catal. Today* **2007**, *120*, 311.
(18) Natesakhawat, S.; Culp, J. T.; Matranga, C.; Bockrath, B. *J Phys. Chem. C* **2007**, *111*, 1055.
(19) Kaye, S. S.; Long, J. R. *Chem. Commun.* **2007**, 4486.
(20) Culp, J. T.; Natesakhawat, S.; Smith, M.; Bittner, E. W.; Matranga, C.; Bockrath, B. *J. Phys. Chem.* **2008**, *112*, 7079.
(21) Reguera, L.; Balmaseda, J.; del Castillo, L. F.; Reguera, E. *J. Phys. Chem. C* **2008**, *112*, 5589.
(22) Reguera, L.; Balmaseda, J.; Krap, C. P.; Reguera, E. *J. Phys. Chem. C* **2008**, *112*, 10490.
(23) Reguera, L., Krap, C. P., Balmaseda, J., Reguera, E. *J. Phys. Chem. C* **2008**, *112*, 15893.
(24) Culp, J. T.; Natesakhawat, S.; Smith, M. R.; Bittner, E.; Matranga, C.; Bockrath, B. *J. Phys. Chem. C* **2008**, *112*, 7079.
(25) Gravereau, P.; Garnier, E. *Rev. Chim. Mineral.* **1983**, *20*, 68.
(26) Rodriguez-Carvajal, J. *FullProf Program*; Institute Louis Brillouin: Saclay, France, 2005.
(27) Bering, B. P.; Serpinskii, V. V. *Izv. Akad. Nauk, Ser. Khim.* **1974**, *11*, 2427.
(28) Rouquerol, F.; Rouquerol, J.; Sing, K. *Adsorption by Powders and Solids: Principles, Methodology and Applications*; Academic Press: London, 1999.
(29) Dubinin, M. M. In *Progress in Surface Science and Membrane Science*; Cadenheat, D. A., Ed.; Academic Press: New York, 1975.
(30) Rodríguez-Hernández, J.; Reguera, E.; Lima, E.; Balmaseda, J.; Martínez-García, R.; Yee-Madeira, H. *J. Phys. Chem. Solids* **2007**, *68*, 1630.
(31) Gravereau, P.; Garnier, E.; Hardy, A. *Acta Crystallogr. B* **1979**, *35*, 2843.
(32) Garnier, E.; Gravereau, P.; Hardy, A. *Acta Crystallogr. B* **1982**, *38*, 1401.
(33) Lima, E.; Balmaseda, J.; Reguera, E. *Langmuir* **2007**, *23*, 5752.
(34) Martínez-García, R.; Knobel, M.; Reguera, E. *J. Phys. Chem. B* **2006**, *110*, 7296.
(35) Rodríguez-Hernández, J.; Gómez, A.; Reguera, E. *J. Phys. D: Appl. Phys.* **2007**, *40*, 6076.
(36) Nakamoto, K. *Infrared and Raman Spectra Inorganic and Coordination Compounds: Applications in Coordination, Organometallic, and Bioinorganic Chemistry*, 5th ed.; John Wiley & Sons: New York, 1997.
(37) Ferlay, S.; Mallah, T.; Ouahes, R.; Veillet, P.; Verdaguer, M. *Nature* **1995**, *378*, 701.
(38) Verdaguer, M.; Bleuzen, A.; Marvaud, V.; Vaissermann, J.; Seuleiman, M.; Desplanches, C.; Scuiller, A.; Train, C.; Garde, R.; Gelly, G.; Lomenech, C.; Rosenman, I.; Veillet, P.; Cartier, C.; Villain, F. *Coord. Chem. Rev.* **1999**, *190−192*, 1023.
(39) Martínez-García, R.; Knobel, M.; Reguera, E. *J. Phys.: Condens. Matter* **2006**, *18*, 11243.
(40) Roque-Malherbe, R. *Adsorption and Diffusion in Nanoporous Materials*; CRC Press, Taylor & Francis Group: Boca Raton, London, NY, 2007.
(41) Holmes, S. M.; Girolami, G. S. *J. Am. Chem. Soc.* **1999**, *121*, 5593.

JP802764V